Hallervorden-Spatz disease: MR and pathologic findings.

M Savoiardo, W C Halliday, N Nardocci, L Strada, L D'Incerti, L Angelini, V Rumi and J D Tesoro-Tess

AJNR Am J Neuroradiol 1993, 14 (1) 155-162
http://www.ajnr.org/content/14/1/155

Hallervorden-Spatz Disease: MR and Pathologic Findings

Mario Savoiardo,[1] William C. Halliday,[2] Nardo Nardocci,[3] Liliana Strada,[1] Ludovico D'Incerti,[1] Lucia Angelini,[3] Viviana Rumi,[3] and John D. Tesoro-Tess[4]

PURPOSE: To compare the MR findings of eight cases with clinical diagnosis of Hallervorden-Spatz disease (HSD) with the pathologic findings of two other cases of HSD. **MATERIALS AND METHODS:** The eight imaged cases were studied with 0.5-T (seven cases) and/or 1.5-T (five cases) units. Six patients also had CT scans. The two other cases with proven HSD had detailed histologic evaluation. **RESULTS:** The 1.5-T findings showed abnormalities confined to the pallidum, which presented a diffuse low signal intensity in T2-weighted images, and an anteromedial area of high signal intensity (eye-of-the-tiger sign). In 0.5-T studies, low signal intensity was less evident and poorly detectable in spin echo, but gradient-echo images could enhance its demonstration; the area of high signal intensity was always well demonstrated. In three cases (three with 1.5 T, one with 0.5 T) a central spot of low signal intensity was seen in this area. The pathologic cases, in addition to neuroaxonal swellings and iron deposits, exhibited areas of "loose" tissue with vacuolization and lesser amounts of iron in the anteromedial part of the pallidum, in a location corresponding to the area of high signal intensity of the imaged cases. **CONCLUSION:** Comparison of MR findings with the pathologic studies demonstrates that the low signal intensity in T2-weighted images at 1.5 T corresponds to iron deposits in a dense tissue, and that the high signal intensity of the eye-of-the-tiger sign corresponds to an area of loose tissue with vacuolization. No correlation was found in the two pathologic cases for the central spot of low signal intensity.

Index terms: Hallervorden-Spatz disease; Degenerative brain disease; Basal ganglia, magnetic resonance

AJNR 14:155–162, Jan/Feb 1993

Hallervorden-Spatz disease (HSD) is a rare neurologic disorder characterized by progressive dystonia, with oromandibular involvement, mental deterioration, pyramidal signs, and retinal degeneration (1). Both familial and sporadic cases have been reported (2–4).

No biologic markers have been found in HSD. HSD is part of the neuroaxonal dystrophies (5, 6), but the diagnosis of HSD can not be obtained by skin or conjunctival biopsy, as in other neuroaxonal dystrophies (5–7).

The characteristic pathologic findings of HSD are the presence of iron deposits in the globus pallidus and neuroaxonal swellings. Therefore, since iron can be detected by high field intensity magnetic resonance (MR) imaging, the possibility of diagnosis in vivo by imaging studies could be expected. In fact, a few reports have already shown some of the characteristic MR findings of HSD (8–15).

Our series of MR studies of eight cases clinically diagnosed as HSD points out the distribution of the MR abnormalities in the pallidum at intermediate and high field intensity.

Since no pathologic studies are available from our series, the MR abnormalities were compared to a detailed pathologic study obtained at another institution on two patients with proven HSD.

Materials and Methods

Of 10 patients clinically diagnosed with HSD at our Institute, eight could be submitted to MR studies. The

Received October 21, 1991; revision requested January 9, 1992; final revision received April 15 and accepted April 17.

[1] Department of Neuroradiology, Istituto Nazionale Neurologico "C. Besta," Via Celoria 11, 20133 Milano, Italy. Address reprint requests to Mario Savoiardo.

[2] Department of Pathology, Section of Neuropathology, Health Sciences Centre and University of Manitoba, 820 Sherbrook Street, Winnipeg, Manitoba R3A 1R9, Canada.

[3] Department of Pediatric Neurology, Istituto Nazionale Neurologico "C. Besta," Via Celoria 11, 20133 Milano, Italy.

[4] Department of Diagnostic Radiology E, Istituto Nazionale dei Tumori, Via Venezian 1, 20133 Milano, Italy.

AJNR 14:155–162, Jan/Feb 1993 0195-6108/93/1401-0155

TABLE 1: Clinical features in the eight imaged patients with HSD

Patient	Sex	Age (yr)	Disease Duration (yr)	Familiarity	Generalized Dystonia	Oromandibular Dystonia	Pyramidal Signs	Retinal Degeneration	Mental Impairment
1	M	26	16	Yes	Yes	+++	Yes	Yes	+++
2	M	12	1	Yes	Yes	+	No	Yes	+
3	M	17	11	Yes	Yes	+++	Yes	Yes	+++
4	F	10	3	Yes	Yes	++	No	Yes	+
5	F	12	10	Yes	Yes	+++	Yes	Yes	+++
6	F	19	5	Yes	Yes	++	Yes	Yes	++
7	M	17	7	No	Yes	+++	Yes	Yes	++
8	M	9	5	No	Yes	+++	Yes	Yes	+

Note:—+ = mild; ++ = moderate; +++ = severe.

remaining two patients (a brother of cases 1 and 2, and a sister of case 5) could not be examined because of the severity of dystonia.

Clinical diagnosis was obtained through clinical history, neurologic examination, exclusion of other possible dystonic disorders by appropriate laboratory tests, and follow-up (16). Disease duration at the moment of first MR studies ranged from 1 to 15 years.

MR studies were performed with a 0.5-T scanner in seven cases and with a 1.5-T unit in five cases.

All the 1.5-T studies included sagittal spin echo (SE) T1-weighted images (TR/TE 200-450/17-35) and axial SE images with long TR and short and long TE (2000/23-100), with 5-mm thickness. In all cases, similar SE coronal images were available. In one case, axial T2* gradient-echo images were obtained (TR/TE/pulse angle 300/18/20°).

The 0.5-T studies included sagittal SE (350-450/30) or gradient-echo (400-450/17-18/90°) T1-weighted images, and axial SE intermediate and T2-weighted images (2000-2200/50-100) of 5- to 7-mm thickness. Intermediate and T2-weighted SE coronal images were also available in all cases. In addition, coronal or axial T1-weighted SE and/or gradient-echo images were performed. In four cases, T2*-weighted images were also obtained (680/25/15°).

In six cases, computed tomography (CT) studies were also available.

The pathologic specimens that were compared with our MR studies were obtained from two cases from another institution. The pathologic cases will be referred to as cases P1 and P2. The first case, a 9-year-old girl, had a progressive neurologic disorder beginning in early infancy. CT scan at age 5 demonstrated a small calcification in the right basal ganglia. The second patient, a woman who died at 31 years of age in a mental institution, also had onset of her disease in early infancy.

The brains of these two patients were sampled widely and the basal ganglia were submitted, in toto, for paraffin embedding and step-sectioning. Five-micron sections were prepared at each 1.5 mm and, at each level, slides were stained with hematoxylineosin (H&E), solochrome cyanine, Bielschowsky, Prussian blue (iron), von Kossa (calcium), and phosphotungstic acid hematoxylin (PTAH) stains. Finally, selected slides were immunocytochemically stained, using the streptavidin-biotin method, for neurofilaments and glial fibrillary acidic protein.

Results

Clinical Aspects of Imaged Cases

The essential clinical data of our eight cases are summarized in Table 1.

The familial cases were two brothers (cases 1 and 2), a brother and a sister (cases 3 and 4), and cases 5 and 6, which came from two different families in which there was history of HSD.

The parents of the familial cases 1 to 5 were examined with MR and found to be normal.

Neuroradiologic Findings

CT. In four of six cases, CT demonstrated high densities consistent with calcifications in the medial part of the pallidum (Table 2). These high densities were tiny and symmetrical in two cases (Fig. 1A), slightly larger in another patient (case 3); in one case, tiny high densities were visible only on the right side. There were no abnormal densities in the rest of the pallidum nor in other areas of the brain.

MR. MR demonstrated somewhat different findings in 1.5-T and 0.5-T studies. At both field strengths, abnormalities were confined to the pallidum (Table 2).

In 1.5-T studies, the most striking finding, seen in all cases, was very low signal intensity with very sharp margins in the pallidum, in T2-weighted images (Fig. 2A). However, in the central or anteromedial part of the pallidum there was always an area of high signal intensity (Figs. 2B and 3B), which sometimes was more evident in proton density images and partly obscured in

TABLE 2: Pallidal abnormalities in eight patients with HSD

Case No.	Sex	Age	CT	MR									Duration of the Disease at Time of Examination (yr)		
				0.5 T					1.5 T					MR	
				T1 SE	T1 GE	PD SE	T2 SE	T2* GE	T1 SE	T1 GE	PD SE	T2 SE	T2* GE	CT	0.5 T	1.5 T
1	M	26	N		↓	↓et	↓↓et	↓↓et						8	15	
2	M	12	Not performed		N	↓et	↓et	↓et							1	
3	M	17	Calcifications bilateral	↓	↓↓	↓	↓et		↓		‖et ↓↓cs	‖‖et ↓↓↓cs		8	9	8
4	F	10	Not performed	↓	↓↓	↓et	↓et		↓		↓et	↓↓↓et			1	2
5	F	12	N	N N	N	et et	|et ↓et							7	8–10	
6	F	19	Calcifications right	↓	↓↓	et cs	|et ↓cs	‖et ↓↓cs	↓		|et ↓cs|	‖‖et ↓↓↓cs		5	5	5
7	M	17	Calcifications bilateral						↓		|et ↓cs	‖‖et ↓↓↓cs		4		4
8	M	9	Calcifications bilateral		↓	↓et	↓et	↓↓et	↓		↓et	↓↓et	↓↓↓et	4	4	4

Note:—N = normal; ↓ = mildly; ↓↓ = moderately; ↓↓↓ = markedly decreased signal intensity; et = eye-of-the-tiger sign; cs = central spot of hypointensity.

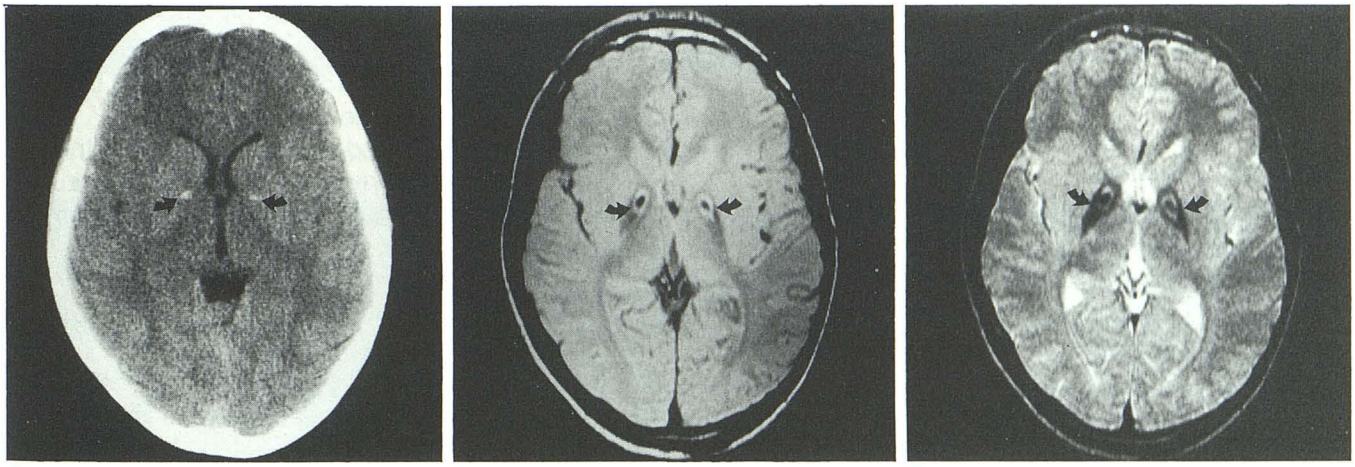

A B C

Fig. 1. Case 7.

A, CT scan shows tiny areas of increased density consistent with calcifications in the internal segment of the pallidum (*arrows*).

B and *C*, MR 1.5-T SE sequence (2000/28-100) in axial section shows marked pallidal hypointensity in T2-weighted image consistent with iron deposits and a central spot of hypointensity within the hyperintense "eye-of-the-tiger" sign (*arrows*).

T2-weighted images. Within this area, in three cases, there was a central spot of very low signal intensity (Figs. 1B and 1C).

In 0.5-T studies, the signal intensity of the greatest part of the pallidum was normal in SE T2-weighted images. However, the high signal intensity in the central or anteromedial part of the pallidum was always evident (Fig. 3A). In one case, the central spot of low signal intensity seen with the 1.5-T was evident also in the 0.5-T study.

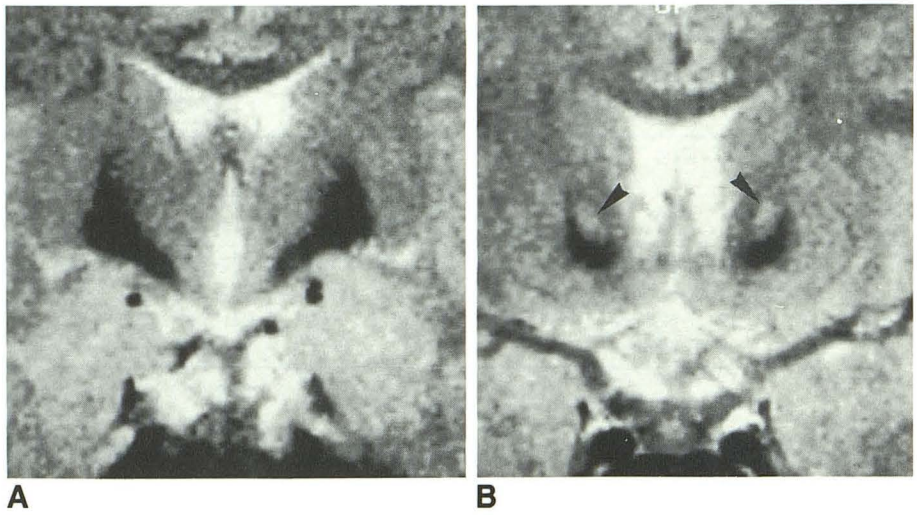

Fig. 2. Case 4; MR 1.5-T. *A* and *B*, Coronal sections, SE 2000/90, show marked pallidal hypointensity with an area of increased signal intensity in the anteromedial part of the pallidum (*B*, *arrowheads*).

The magnetic susceptibility effect of iron was enhanced in two cases, giving lower signal intensity, in T2*-weighted, gradient-echo images. However, the difference in pallidal signal intensity between SE and gradient-echo images was more evident in our cases in T1-weighted images (Fig. 4).

No abnormalities could be demonstrated in the substantia nigra with either 1.5-T or 0.5-T magnets.

Patients with different disease duration did not show differences in signal abnormalities. One patient (case 5), who had two MR examinations 2 years apart, presented only a questionable increase in signal abnormalities.

Pathologic Findings

The fresh brain of case P1 weighed 1280 grams; the major gross pathologic finding was a rusty brown discoloration limited to the globus pallidus. The brain weight of case P2 was 810 grams; both the globus pallidus and the substantia nigra presented a brownish discoloration (Fig. 5A).

On microscopic examination, in both cases, there were innumerable dystrophic axons throughout the globus pallidus (Fig. 5B). In case P1, dystrophic axons were abundant in the pencilate fibers of the caudate nucleus and putamen. This was less evident in case P2. In both cases, but particularly in case P1, two histologic patterns were appreciated in the globus pallidus. The first consisted of a rather "dense" tissue consisting of dystrophic axons, reactive astrocytes, and residual neurons. The second pattern was associated with a rather "loose" tissue in which the above elements were separated by vacuoles (Figs. 6A, 6C, and 6D). In case P2, the dense pattern prevailed.

Mineralization was limited to the globus pallidus and stains for iron were intensely positive (Fig. 6B). Conversely, stains for calcium were negative. Although mineralization of the neuropil occurred throughout the globus pallidus, it was particularly evident in the central regions. Vessels within the globus pallidus showed sclerosis and mineralization (Fig. 6B), particularly in case P2. Immunohistochemical staining for glial fibrillary acidic protein emphasized the gliosis of the pallidum and demonstrated the reactive astrocytes. The dystrophic axons showed a spectrum in their immunopositivity for neurofilaments.

It must be mentioned that an additional finding in case P2 was the presence of abundant neurofibrillary tangles in the neocortex, hippocampus, diencephalon, and brain stem.

Discussion

High densities on CT consistent with calcifications, similar to those observed in our cases, can be observed in Fahr disease (17), in endocrine parathyroid disorders (17), and in mitochondrial encephalomyopathies, like MELAS (18, 19, 20); in these conditions, they are usually coarser than those observed in our cases of HSD. Moreover, the negative stains for calcium of our two pathologic cases suggest that the high densities observed on CT scans in four of our patients could represent iron deposits.

MR at high field intensity has the property of demonstrating iron or other paramagnetic elements because of preferential T2 proton relaxa-

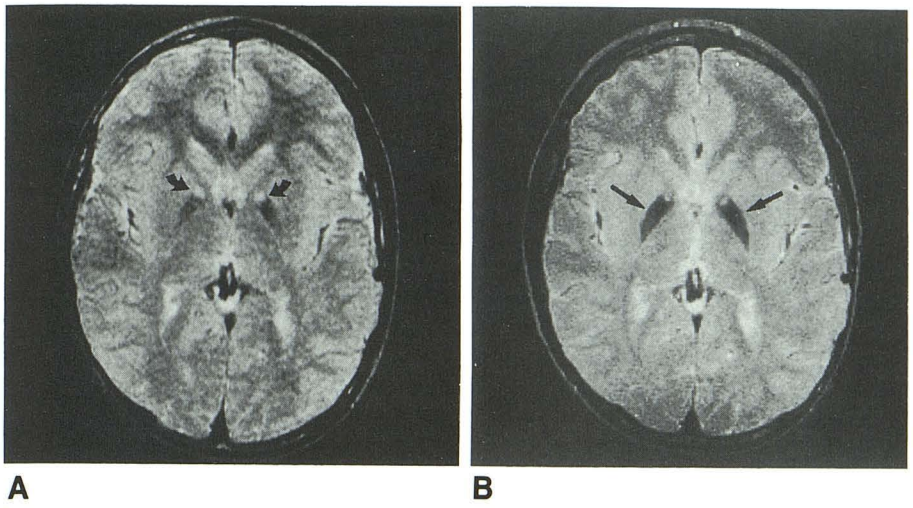

Fig. 3. Case 8: SE T2-weighted images in 0.5-T (*A*, 2100/100) and 1.5-T (*B*, 2000/90) studies. With intermediate field intensity (*A*) the high signal intensity areas are well seen (*arrows*); however, high field intensity is required to demonstrate satisfactorily the magnetic susceptibility effects of iron (*B*) (*arrows*).

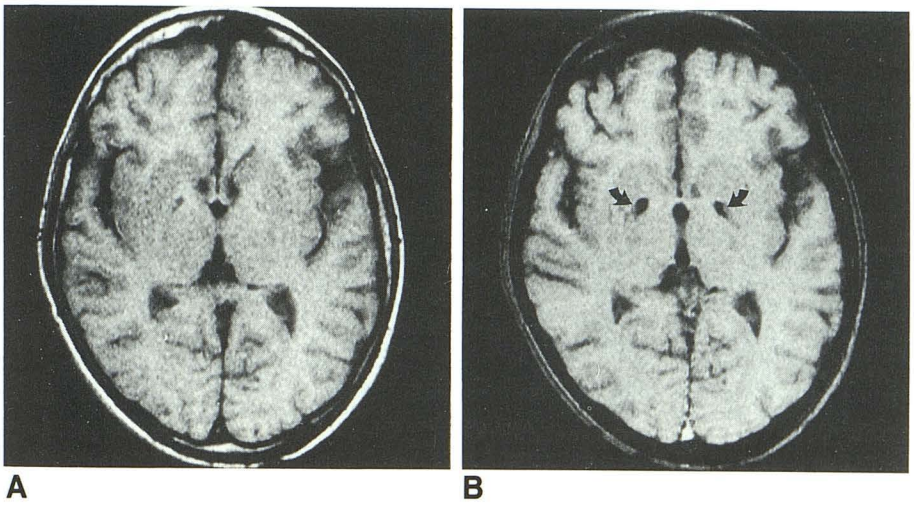

Fig. 4. Case 3: MR 0.5-T, T1-weighted images in SE (350/30, *A*) and gradient-echo (410/18/90°, *B*) sequences; pallidal hypointensity is well-seen only in gradient-echo images (*arrows*).

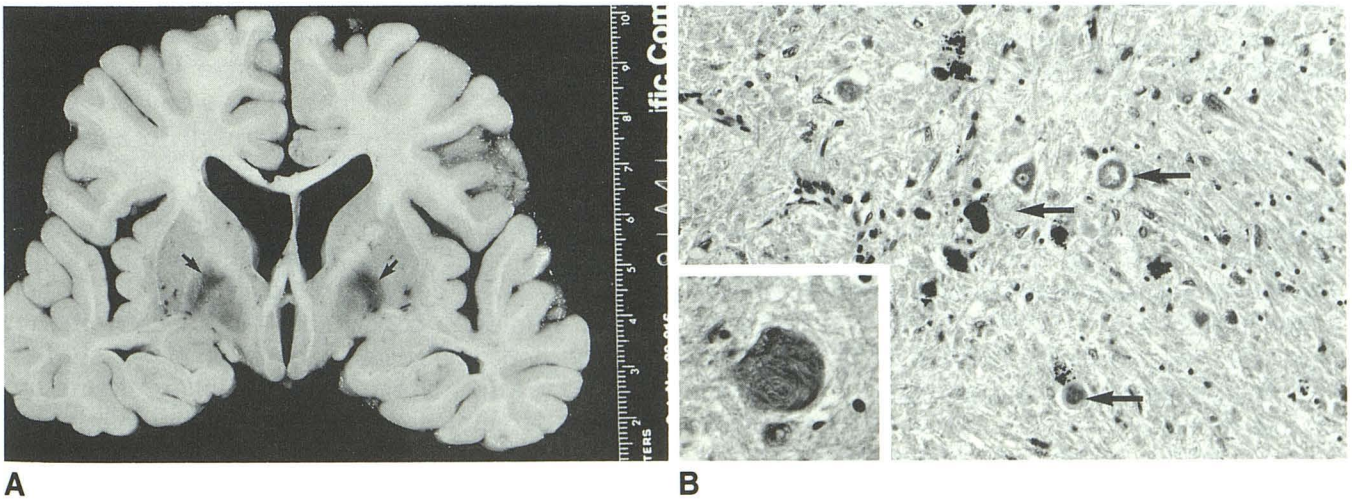

Fig. 5. Case P2.

A, Coronal section of the cerebral hemispheres demonstrates pigmentation of globus pallidus (*arrows*).

B, The globus pallidus contains dystrophic axons (*arrows*), residual neurons, astrocytes, and foci of mineralization. Neurons in the adjacent basal nuclei (inset) frequently contained neurofibrillary tangles. Hematoxylineosin, ×320, inset ×640.

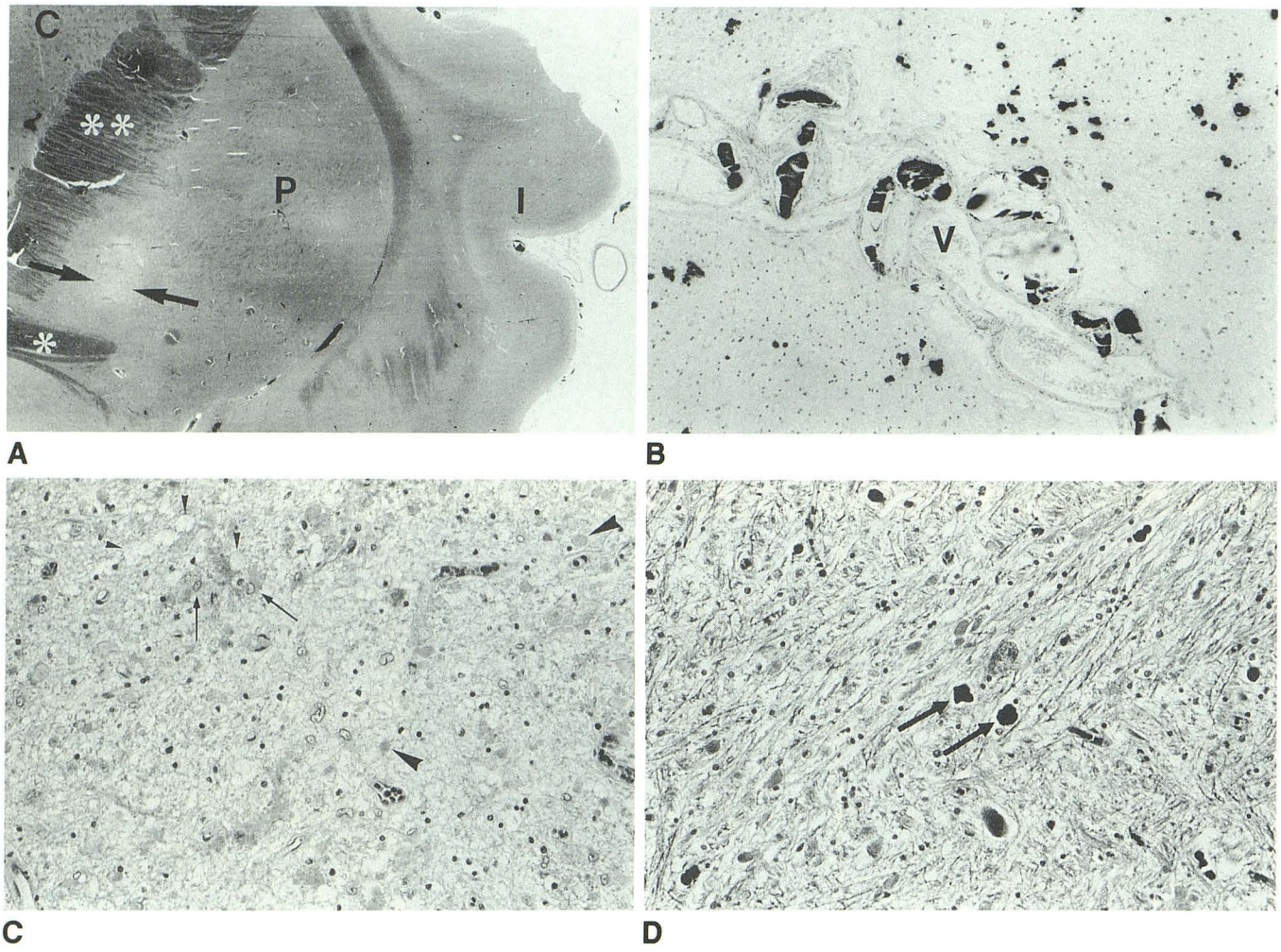

Fig. 6. Case P1.

A, Coronal section of the lenticular nucleus demonstrates a "loose" area (*arrows*) bounded by the anterior commissure (*), internal capsule (**), and putamen (*P*). The caudate nucleus (*C*) and insula (*I*) are identified. Heidenhain's myelin, ×5.5. Compare with Figure 2B.

B, Pallidal iron deposits are found in both the brain tissue and the walls of lenticulostriate vessels (*V*). Perls' Prussian blue, ×160.

C, The "loose" area consists mainly of reactive astrocytes (*arrows*) and dystrophic axons (*large arrowheads*) separated by vacuoles (*small arrowheads*). Hematoxylineosin, ×320.

D, Mineralization (*arrows*) is more evident in the "dense" areas. Hematoxylineosin, ×320.

tion enhancement (11, 21, 22). This magnetic susceptibility effect is proportional to the square of the magnetic field intensity and causes a loss of signal intensity in T2-weighted images (22). MR exquisitely demonstrates the presence of iron in the pallidum in HSD (8–15); in one reported case, the MR-pathologic correlation is presented (14). In this report, MR demonstrates a small area of higher signal intensity within the low signal intensity of the pallidum in T2-weighted images. However, only a few reports emphasize that the signal intensity in the pallidum is not uniformly low, but that there is an area of higher signal intensity in the central or anteromedial part of the globus pallidus (11, 12, 15). This has been called the "eye-of-the-tiger" sign by Sethi et al (12).

The eye-of-the-tiger sign was demonstrated in all of our cases (Figs. 2 and 3). The high signal intensity, well demonstrated in both 1.5-T and 0.5-T studies, is consistent with a lesser amount of iron and high water content. In 0.5-T studies, in which iron magnetic susceptibility effects are poorly detectable, this high signal intensity area within the pallidum could, therefore, suggest HSD.

High signal intensity in the globus pallidus, however, can be observed in a variety of lesions, including ischemia and a few metabolic disorders such as organic acidurias (23). Other disorders

affecting the basal ganglia, such as Leigh disease and other mitochondrial encephalopathies, infantile bilateral necrosis, and Wilson disease, more frequently involve the neostriatum, particularly the putamen, rather than the pallidum (24–27).

In our series of patients with clinical diagnosis of HSD, MR both at high and intermediate field intensity demonstrates pathologic findings confined to the pallidum, suggesting iron deposits in almost the entire nucleus, except for a small area of signal intensity consistent with increased water content.

The pathologic reports of HSD cases (1, 5, 6, 16, 28) never clearly mention a different distribution of the histologic abnormalities within the pallidum. Only Dooling et al (2) stated that gliosis and destructive changes tend to occur mostly in the internal segment of the pallidum.

The histologic findings of the pathologically proved cases here reported demonstrate that, particularly in case P1, there are areas with different tissue density within the pallidum (Fig. 6). The areas of vacuolization with less abundant iron deposits provide a good explanation for the areas of high signal intensity in T2-weighted images constantly observed in MR studies (compare Fig. 6A with MR studies).

In HSD, the iron in the globus pallidus does not extend beyond its boundaries, and this also corresponds well to the sharp margin of low signal intensity seen in T2-weighted images (Figs. 2A and 3B). If tiny deposits of calcium are present, they are in any case limited to a much smaller area than the deposits of iron, which involve the whole pallidum up to its edges, as demonstrated by the extent of the magnetic susceptibility effects observed on MR (Fig. 1).

In spite of the good correspondence between the MR features and the pathologic findings of HSD cases, a few clinical and imaging problems regarding the specificity of diagnosis of HSD remain. Other neuroaxonal dystrophies, with a somewhat different clinical presentation from that of our HSD cases, present the same pathologic abnormalities in the globus pallidus, as reported by Dooling et al (2) and Eidelberg et al (28). The central spot of hypointensity seen in three of our cases within the hyperdense area in the anteromedial part of the pallidum (Fig. 1) was not seen in any other case reported in the literature that we reviewed nor was it found to have a correlate in the two pathologic cases we studied.

Acknowledgments

We thank Dr S. Seshia, pediatric neurologist, Winnipeg, for the clinical evaluation of the first pathologic case; without his considerable efforts the pathologic study would not have been possible.

References

1. Wigboldus JM, Bruyn GW. Hallervorden-Spatz disease. In: Vinken PJ, Bruyn, GW, eds. *Handbook of clinical neurology: diseases of basal ganglia.* Vol 6. Amsterdam: North Holland, 1968:604–631
2. Dooling EC, Schoene WC, Richardson EP Jr. Hallervorden-Spatz syndrome. *Arch Neurol* 1974;30:70–83
3. Elejalde BR, DeElejalde MD, Lopez F. Hallervorden-Spatz disease. *Clin Genet* 1979;16:1–18
4. Vakili S, Drew AL, Von Schuching S, Becker D, Zeman W. Hallervorden-Spatz syndrome. *Arch Neurol* 1977;34:729–738
5. Seitelberger F, Jellinger K. Neuroaxonal dystrophy and Hallervorden-Spatz disease. In: Goldensohn ES, Appel SM, eds. *Scientific approaches to clinical neurology.* Vol II. Philadelphia: Lea & Febiger, 1977:1052–1072
6. Seitelberger F. Neuroaxonal dystrophy: its relation to aging and neurological diseases. In: Vinken PJ, Bruyn GW, Klawans HL, eds. *Handbook of clinical neurology: extrapyramidal disorders.* Vol. 49. New York: Elsevier, 1986:391–413
7. Defendini R, Markesbery WR, Mastry AR, Duffy PE. Hallervorden-Spatz disease and infantile neuroaxonal dystrophy. Ultrastructural observations, anatomical pathology and nosology. *J Neurol Sci* 1973;20:7–23
8. Littrup PJ, Gebarski SS. MR imaging of Hallervorden-Spatz disease. *J Comput Assist Tomogr* 1985;9:491–493
9. Tanfani G, Mascalchi M, Dal Pozzo GC, Taverni N, Saia A, Trevisan C. MR imaging in a case of Hallervorden-Spatz disease. *J Comput Assist Tomogr* 1987;11:1057–1058
10. Mutoh K, Okuno T, Ito M, et al. MR imaging of a group I case of Hallervorden-Spatz disease. *J Comput Assist Tomogr* 1988;12:851–853
11. Rutledge JN, Hilal SK, Silver AJ, Defendini R, Fahn S. Study of movement disorders and brain iron by MR. *AJNR* 1987;8:397–411
12. Sethi KD, Adams RJ, Loring DW, El Gammal T. Hallervorden-Spatz syndrome: clinical and magnetic resonance imaging correlations. *Ann Neurol* 1988;24:692–694
13. Gallucci M, Cardona F, Arachi M, Splendiani A, Bozzao A, Passariello R. Follow-up MR studies in Hallervorden-Spatz disease. *J Comput Assist Tomogr* 1989;14:118–120
14. Schaffert DA, Johnsen SD, Johnson PC, Drayer BP. Magnetic resonance imaging in pathologically proven Hallervorden-Spatz disease. *Neurology* 1989;39:440–442
15. Ambrosetto P, Nonni R, Bacci A, Gobbi G. Late onset familial Hallervorden-Spatz disease: MR findings in two sisters. *AJNR* 1992;13:394–396
16. Fahn S, Marsden CD, Calne DB. Classification and investigation of dystonia. In: Marsden CD, Fahn S, eds. *Movement disorders 2.* London: Butterworth, 1987:332–358
17. Cohen CR, Duchesneau PM, Weinstein MA. Calcification of the basal ganglia as visualized by computed tomography. *Radiology* 1980; 134:97–99
18. Allard JC, Tilak S, Carter AP. CT and MR of MELAS syndrome. *AJNR* 1988;9:1234–1238
19. Hasuo K, Tamura S, Yasumori K, et al. Computed tomography and angiography in MELAS (mitochondrial myopathy, encephalopathy, lactic acidosis and stroke-like episodes): report of 3 cases. *Neuroradiology* 1987;29:393–397
20. Pavlakis SG, Phillips PC, Di Mauro S, De Vivo DC, Rowland LP.

Mitochondrial myopathy, encephalopathy, lactic acidosis, and stroke-like episodes: a distinctive clinical syndrome. *Ann Neurol* 1984; 16:481–488

21. Drayer B, Burger P, Darwin R, Riederer S, Herfkens R, Johnson GA. Magnetic resonance imaging of brain iron. *AJNR* 1986;7:373–380
22. Gomori JM, Grossman RI, Goldberg HI, Zimmerman RA, Bilaniuk LT. Intracranial hematomas: imaging by high-field MR. *Radiology* 1985; 157:87–93
23. Van der Knaap MS, Valk J, de Neeling N, Nauta JJP. Pattern recognition in magnetic resonance imaging of white matter disorders in children and young adults. *Neuroradiology* 1991;33:478–493
24. Savoiardo M, Uziel G, Strada L, Visciani A, Grisoli M, Wang G. MRI findings in Leigh's disease with cytochrome-*c*-oxidase deficiency. *Neuroradiology* 1991;33(suppl):507–508
25. Savoiardo M, Passerini A, D'Incerti L. Neuroradiology of basal ganglia diseases in children and adolescents. In: Angelini L, Lanzi G, Balottin U, Nardocci N, eds. *Extrapyramidal disorders in childhood.* New York: Excerpta Medica, 1987:151–167
26. Leuzzi V, Bertini E, De Negri AM, Gallucci M, Garavaglia B. Bilateral striatal necrosis, dystonia and optic atrophy in two siblings. *J Neurol Neurosurg Psychiatry* 1992;55:16–19
27. Prayer L, Wimberger D, Kramer J, Grimm G, Oder W, Imhof H. Cranial MRI in Wilson's disease. *Neuroradiology* 1990;32:211–214
28. Eidelberg D, Sotrel A, Joachim C, et al. Adult onset Hallervorden-Spatz disease with neurofibrillary pathology. *Brain* 1987;110:993–1013